HHS Public Access

Author manuscript

*Nat Methods*. Author manuscript; available in PMC 2013 January 01.

Published in final edited form as:

*Nat Methods*. ; 9(7): 749–754. doi:10.1038/nmeth.2025.

# Resolution Doubling in Live, Multicellular Organisms via Multifocal Structured Illumination Microscopy

**Andrew G. York**[1], **Sapun H. Parekh**[1,5], **Damian Dalle Nogare**[2], **Robert S. Fischer**[3], **Kelsey Temprine**[1], **Marina Mione**[4], **Ajay B. Chitnis**[2], **Christian A. Combs**[3], and **Hari Shroff**[1]

[1] Section on High Resolution Optical Imaging, National Institute of Biomedical Imaging and Bioengineering, National Institutes of Health, Bethesda, MD 20892

[2] National Institute of Child Health and Human Development, National Institutes of Health, Bethesda, MD 20892

[3] National Heart, Lung, and Blood Institute Light Microscopy Facility, National Institutes of Health, Bethesda, MD 20892

[4] Institute of Toxicology and Genetics, Karlsruhe Institute of Technology, Karlsruhe, Germany

## Abstract

We demonstrate 3D super-resolution in live multicellular organisms using structured illumination microscopy (SIM). Sparse multifocal illumination patterns generated by a digital micromirror device (DMD) let us physically reject out-of-focus light, enabling 3D subdiffractive imaging in samples 8-fold thicker than previously demonstrated with SIM. We imaged a variety of samples at one 2D image per second, at resolutions down to 145 nm laterally and 400 nm axially. In addition to dual-labeled, whole fixed cells, we imaged GFP-labeled microtubules in live transgenic zebrafish embryos at depths greater than 45 μm. We also captured dynamic changes in the zebrafish lateral line primordium and observed the interactions between myosin IIA and F-actin in cells encapsulated within collagen gels, obtaining two-color 4D super-resolution datasets spanning tens of time points and minutes without apparent phototoxicity. Our method uses commercially available parts and open-source software and is simpler than existing SIM implementations, allowing easy integration with widefield microscopes.

The 100-fold mismatch in size between the resolution of an optical microscope and the length scales of biomolecular complexes hinders direct observation of subcellular phenomena. Imaging beyond the diffraction limit is thus of great practical interest in cell biology, and the last decade has seen an explosion in ‘super-resolution’ optical imaging



Correspondence should be addressed to A.G.Y. (andrew.g.york+naturemethods@gmail.com).

[5]Present Address: Molecular Spectroscopy Department, Max-Planck-Institute for Polymer Research, 55128 Mainz, Germany

Author contributions

A.G.Y. and H.S. conceived the idea. A.G.Y., S.H.P., C.A.C. and H.S. designed and built the experimental setup. A.G.Y. and S.H.P. wrote the analysis code and performed simulations. A.G.Y., S.H.P., D.D.N., R.S.F., C.A.C., and H.S. took the data. A.G.Y., S.H.P., D.D.N, R.S.F., K.T., A.B. C., C.A.C., and H.S. analyzed the data. S.H.P., D.D.N., R.S.F, and K.T. prepared samples. M.M., A.B. C., and C.A.C. contributed reagents and materials. A.G.Y., S.H.P., D.D.N., R.S.F., and H.S. wrote the paper with input from all authors. H.S. designed and supervised research.

techniques[1]. Despite these advances, long-term live imaging of thick samples still presents challenges for such methods.

Photoactivated localization microscopy (PALM)[2] and related single-molecule imaging techniques[3,4] enable imaging with lateral resolutions down to 20 nm (sub-100 nm axially) on 3D samples such as whole fixed cells[5,6] and much thicker cellular spheroids[7]. While a few live cell experiments have been performed at slow imaging rates over extended durations[8] and at rates up to 2 Hz for very short periods[9], the current requirements for ~kW/cm$^2$ excitation intensities and thousands of frames have confined most efforts to fixed cells.

Stimulated emission depletion microscopy[10] (STED) enables cellular imaging with ~20-100 nm resolution[11]. STED has also been applied to thicker samples[12,13], although so far only providing 2D super-resolution. STED resolution scales with illumination intensity, constraining the choice of dyes and entailing a compromise between spatial resolution and phototoxicity in live experiments.

In structured illumination microscopy (SIM)[14,15], spatially patterned light is used to excite sample fluorescence. Frequency-mixing between the excitation pattern and fluorophore density moves normally unobservable high resolution information in the sample into the observable passband of the microscope. By varying the pattern orientation and phase, recording the resulting fluorescence, and appropriately post-processing the resulting multi-image datasets, it is possible to obtain images with ~100 nm lateral and ~300 nm axial resolution[16] for linear SIM. While this resolution is more modest than that of PALM or STED, SIM offers other advantages. The number of raw images required for a single SIM image is far fewer than in PALM, and the illumination intensity is far less than in STED. These benefits allow increased imaging speed and duration, and enable live SIM at 11 Hz in 2D[17] and 0.2 Hz in 3D on whole cells[18] for hundreds of time points. Linear SIM is also compatible with the full array of conventional fluorescent dyes, unlike PALM or STED.

In addition to resolution-doubling, 3D SIM offers another major advantage over conventional widefield imaging: computational optical sectioning (the removal of out-of-focus blur). While highly effective on thin samples, SIM retains the shot noise associated with the computationally removed background, and is unsuitable for thick or very densely-labeled samples. Confocal microscopy physically rejects out-of-focus light with a pinhole, and provides higher contrast images in thick samples. Confocal microscopes, however, provide at best a √2 improvement in lateral resolution with a small pinhole, and this enhanced resolution is difficult to attain as the corresponding loss in signal is prohibitive.

We present a hybrid technique, multifocal SIM (MSIM), that combines the resolution-doubling characteristics of SIM with the physical optical sectioning of confocal microscopy. MSIM uses sparse 2D excitation patterns generated with a digital micromirror device (DMD) integrated into a conventional wide-field microscope and digital post-processing to obtain optically-sectioned images with ~145 nm lateral and ~400 nm axial resolution at 1 Hz frame rates. Relative to existing SIM, our implementation is easier to integrate onto existing microscopes and is considerably cheaper than commercial SIM. We obtain dual-color,

volumetric images of whole fixed cells, and extend SIM to live samples 8-fold thicker than previous experiments on whole cells. We apply 4D MSIM to study the evolution of the posterior lateral line primordium in live zebrafish embryos and also obtain multicolor, 4D super-resolution datasets on cells embedded in collagen gels.

## Results

Using point-like illumination for SIM has been explored in image scanning microscopy (ISM)[19]. In ISM, a focused beam excites fluorescence, which is imaged through a confocal pinhole and recorded onto a camera. The excitation beam is rastered through the sample, and an image is recorded for each position of the beam. An image with √2 improvement in spatial resolution is obtained by scaling (2x) and summing the raw images, a process analogous to stopping down the pinhole in confocal microscopy (**Supplementary Note 1** and **Supplementary Fig. 1**). Deconvolution further increases the ISM resolution to 150 nm laterally, a 1.63-fold improvement over the raw data.

ISM offers the sectioning capability of a confocal microscope and has better resolution and no trade-off in signal-to-noise ratio (SNR) The weakness of ISM is its speed. Recording a single 2D image at each illumination location is far too slow for monitoring many live cellular processes. Covering a relatively small ~2 μm field of view at the required step size (40 nm), even at fast frame rates (100 Hz) results in a total acquisition time of 25 s. Larger fields would take proportionately more time.

We reasoned that parallelization of ISM by using a sparse lattice of excitation foci (similar to swept-field or spinning disk confocal microscopy) would dramatically increase speed. After excitation by this multifocal pattern and fluorescent readout, the multifocal pattern is translated, and this procedure is repeated until the entire field of view has been illuminated. Post-processing (pinholing, 2x scaling, and summing) gave a reconstructed image with better resolution and less out-of-focus haze than a widefield image. This reconstruction may be further processed by deconvolution to yield a resolution-doubled MSIM image (**Supplementary Fig. 2**, **Supplementary Video 1**, and **Online Methods**).

### MSIM Implementation

We chose a commercially available DMD (**Supplementary Note 2**) to generate and switch multifocal patterns, due to its comparatively low cost and high switching speed (> 20 kHz). Each illumination spot was created by a single DMD mirror pixel in the ‘ON’ position. Our illumination optics demagnified each 10.8 μm × 10.8 μm DMD pixel by 90x to 120 nm × 120 nm in the sample (**Supplementary Fig. 3**), generating illumination foci limited by diffraction and aberrations. Additional demagnification did not improve resolution, but reduced excitation transmission efficiency.

We chose a periodic lattice of approximately equilateral triangles for our illumination locations, because this pattern maximizes the distance between any two nearest neighbors for a given density of points (reducing crosstalk between points while minimizing the number of translations required to cover the field). We translated this multifocal pattern by one DMD pixel at a time, corresponding to a step size of 120 nm in the sample plane. Larger

steps did not evenly illuminate the sample, giving a visible striping artifact, while smaller steps increased acquisition time and dose with no improvement in image quality.

Multifocal excitation patterns were imaged onto the sample mounted in a commercial, inverted microscope, and a scientific-grade complementary metal-oxide-semiconductor (sCMOS) camera, (**Supplementary Note 3**) recorded one raw image per pattern position. Varying the spacing between the illumination points trades acquisition speed for sectioning quality. Widely spaced foci had less crosstalk, but more patterns were required to evenly illuminate the sample. Denser foci had more crosstalk, but required correspondingly fewer patterns (**Supplementary Fig. 4**). We found that 16 pixel horizontal and 14 pixel vertical separation between scan points gave good results in the samples we investigated. The resulting 224 raw exposures taken at 222 Hz (for our 480 pixel × 480 pixel field of view) corresponded to a ~1 Hz super-resolution image acquisition rate. Pinholing, scaling, summing, and deconvolution (**Supplementary Note 4**) were applied after acquisition to generate MSIM images. For pinholing, we used a Gaussian mask with $\sigma = 162$ nm centered on each illumination focus to remove out of focus haze (**Supplementary Fig. 5**).

## Resolution Doubling in Biological Samples

To investigate MSIM's potential for biological imaging, we imaged antibody-labeled microtubules in human osteosarcoma (U2OS) cells embedded in Fluoromount (**Fig. 1a**). Compared to widefield images, the multifocal-excited, pinholed, scaled, and summed (MPSS) images improved resolution and contrast (**Fig. 1b,c**). Iterative deconvolution further improved MPSS images, revealing features obscured by diffraction (**Fig. 1b,c**). The same deconvolution failed to improve the resolution of widefield images appreciably (**Supplementary Fig. 6**). The apparent full width at half maximum (FWHM) intensity of microtubules in MSIM images was 145 nm, a 2-fold improvement compared to widefield imaging (**Fig. 1d**). Similar experiments on 110 nm beads confirmed this result (MSIM FWHM 146 ± 15 nm vs. widefield FWHM 284 ± 32 nm, $N = 80$ beads, **Supplementary Fig. 7**). The acquisition time for the 48 μm × 49 μm field (**Fig. 1a**) was ~1 s, more than a 6500-fold improvement over ISM, assuming the same 222 Hz raw frame rate.

We next investigated our technique's suitability for 3D, dual-labeled samples by acquiring a Z stack of MSIM images on a fixed cell embedded in Fluoromount **(Fig. 2**). We immunolabeled microtubules with Alexa Fluor 488 and stained mitochondria with Mitotracker Red, obtaining a 3 μm thick volume with slices separated by 100 nm **(Fig. 2a** and **Supplementary Video 2)**. Compared to widefield images 3D MSIM provided a striking increase in image contrast, due to the combined physical (via the digital pinholes) and computational (via 3D deconvolution) removal of out-of-focus light (**Fig. 2b** and **Supplementary Videos 2** and **3)**.

MSIM images retained two-fold lateral resolution improvement over widefield imaging, better resolving microtubules and ‘worm-like’ mitochondria. We resolved subdiffractive voids at the ends of individual mitochondria as well as microtubule pairs separated by < 200 nm (**Supplementary Fig. 8**). Unexpectedly, MSIM improved our axial resolution ~2x over widefield. The apparent axial FWHM of microtubules was ~400 nm, a result confirmed on

110 nm beads (MSIM FWHM 402 ± 49 nm, widefield 826 ± 83 nm, *N* = 80 beads, **Supplementary Fig. 7**).

## Extension of MSIM to live, multicellular samples

Previous live SIM is limited to axial depths of ~6 μm, the thickness of a single HeLa cell[18]. MSIM enables 3D imaging of thicker live samples, because pinholing rejects out-of-focus light that would otherwise swamp in-focus signal. To demonstrate this feature, we imaged live, immobilized zebrafish embryos expressing a GFP transgene that labeled microtubules (**Fig. 3** and **Supplementary Videos 4** and **5**).

For MSIM of a 48.2 μm thick volume we acquired 241 slices spaced 0.2 μm apart at a 2D imaging rate of 1 Hz (**Fig. 3a**). Although we did not measure the distance from the coverslip to the sample, 5 sections (1 μm) were present in the stack before the first appearance of GFP signal in the epidermis of the fish. This tissue volume thus ranged from just superficial to the epidermal layer of the fish through an entire somite. Structural features, such as the boundary between two adjacent somites, alignment of microtubules along the somite boundary, and microtubule free-regions corresponding to the nuclei of the developing muscle cells, are clearly visible. Estimating the axial position of nuclei suggests that the imaging volume contains 6-7 cell layers.

We imaged fast enough to capture a dividing cell in the epidermis (**Fig. 3a-c**) without significant motion blur. The resolution enhancement of MSIM was retained throughout the volume, as the separation between microtubule pairs at the site of cell division was resolved to better than 200 nm (**Fig. 3c**), and microtubules in the epidermis had lateral FWHM 175 ± 21 nm (*N* = 30) and axial FWHM 496 ± 65 nm (*N* = 21). This resolution decreased to 195 ± 33 nm laterally (*N* = 30) and 639 ± 88 nm axially (*N* = 21) near the somite boundary (40 μm into the stack), presumably due to depth-dependent aberrations and scattering. Comparative experiments on a confocal microscope at similar NA and acquisition speed revealed similar features in the epidermis and somites, including individual microtubules and the nuclei of developing muscle cells (**Supplementary Video 6**). Although direct comparison between MSIM and confocal microscopy is difficult -- due to differences in objectives, embryos, excitation power, and detection efficiency -- the lateral FWHM of microtubules in the epidermis was 392 nm ± 77 nm (*N* = 21), more than 2x worse than the MSIM resolution at the same depth (**Supplementary Fig. 9**).

## Volumetric time-lapse imaging in live embryos

To explore MSIM's potential for time-lapse, volumetric (4D) imaging in multicellular organisms, we imaged the posterior lateral line primordium (pLLP)[20] in the same zebrafish line **(Fig. 4** and **Supplementary Videos 7-9**). The pLLP is a group of ~100 cells which migrates underneath the epidermis along the trunk of the embryo. During migration, the pLLP periodically deposits apically constricted clusters of epithelial cells (neuromasts) which eventually form the sensory organs of the lateral line. We acquired volumetric images every minute for ~50 minutes (22 slices per volume, spaced 0.6 μm apart, ~40 s between volumes), starting collection 10 μm past the epidermis and imaging through the pLLP (**Fig. 4a** and **Supplementary Video 7**). We resolved microtubules throughout the entire pLLP,

from apical neuromast constrictions to basal cell bodies, a thickness of ~12 μm (**Supplementary Video 8**).

Of particular interest in lateral line biology is the generation and organization of proto-neuromasts within the traveling pLLP. Although much of the underlying signaling has been determined[21,22], the precise mechanisms by which migrating mesenchymal cells organize into centrally oriented cell clusters, or rosettes, with a prominent apical construction remain elusive. The ability to define and follow individual microtubules (resolved to ~150 nm) from cell bodies in the basal portion of the rosette allows precise definition of the structure of a proto-neuromast (**Fig. 4a,b** and **Supplementary Video 9**). Furthermore, the MSIM dataset suggests that mesenchymal cells in the leading part of the pLLP show a prominent apical organization of microtubules at the midline of the migrating pLLP even before incorporation into a proto-neuromast (**Fig. 4b**). This previously undocumented feature may allow for a richer understanding of the transition that initially mesenchymal cells in the leading domain undergo as they assume an epithelial character and are incorporated into the nascent proto-neuromasts.

We also acquired 4D datasets of live, transgenic *C. elegans* embryos expressing GFP-histones (**Supplementary Fig. 10** and **Supplementary Video 10**). Although we were able to recover super-resolution information up to ~10 μm, MSIM images at greater depths exhibited pronounced degradation in SNR and resolution, presumably due to increased scattering or depth-dependent aberrations induced by the sample. These deleterious effects must be addressed before super-resolution can be achieved throughout whole, live nematode embryos.

## Dual-color 4D MSIM in collagen gels

Most single-cell fluorescence microscopy is performed at or near the coverslip, where imaging conditions are benign. However, studies on breast cancer progression[23], metastasis[24], and mesenchymal stem cell differentiation[25] show the 3D environment of cells significantly affects their biology, highlighting the need for high resolution methods suited for imaging away from the coverslip[26]. We demonstrated MSIM's capability for these applications by performing multicolor 4D super-resolution imaging of human osteosarcoma cells invading a collagen matrix, more than 40 μm into the matrix (**Fig. 5** and **Supplementary Video 11**). We acquired sequential two-color volumes (25 slices per volume, 0.2 μm apart, ~60 s between time points, 2D imaging rate 1 Hz) over 26 time points, observing interactions between myosin IIA (labeled with GFP) and actin filaments (labeled with td-Tomato F-tractin) within the invadapodia. Individual actin filament bundles were clearly resolved despite their close proximity (~250 nm), and were decorated with myosin IIA. Along the actin cortex, myosin IIA formed striations with repeat frequency ~350 nm, consistent with previous findings in 2D cell culture[27].

At the invadapodia periphery, we observed highly dynamic filopodia, with apparent diameter ~150-200 nm, consistent with previous observations[28]. Interestingly, as groups or individual filapodia retracted, concentrations of myosin IIA concomitantly appeared, suggesting that local accumulation of myosin IIA at the cortex may cause retraction of filopodia during invasion of 3D matrices. The cell dynamically protruded and retracted

throughout the 50 minute imaging period, suggesting that our excitation intensities did not significantly perturb the observed dynamics.

## Discussion

Like existing 3D SIM[16], MSIM provides resolution doubling by increasing the highest spatial frequencies encoded in the raw data, followed by deconvolution. However, the absolute resolutions we report are slightly lower. We attribute this to two factors. First, achieving the highest possible resolution relies on obtaining diffraction-limited widefield performance before (M)SIM is applied. Although we attempted this, the widefield point spread functions (PSFs) we measured (**Supplementary Fig. 7**) had FWHM (~280 nm) larger than theoretical predictions. It is customary in SIM to screen many objectives and use only the one with highest resolution. We did not do this. Furthermore, we suspect that aberrations caused by warping of the dichroic internal to our microscope was the major cause of departure from ideal performance, as we noticed that small adjustments of the mounting screws that held the dichroic drastically altered the PSF. A thicker, stiffer dichroic may mitigate this issue. Second, the excitation patterns in previous SIM concentrate energy at the very highest lateral spatial frequencies in the objective pass-band. In contrast, the multifocal excitation patterns we used contain all spatial frequencies permitted by the objective. We might thus expect line-excitation based SIM to provide a greater SNR at high spatial frequencies than MSIM, enabling higher resolution. We note the point-like nature of our excitation pattern offers a route to even higher resolution, perhaps by exploiting the nonlinearities provided by reversible, switchable fluorescent probes[29].

Compared to previous SIM, our system is simpler to build. We add only a DMD, a telescope, and a fast camera to a conventional widefield microscope. Our illumination path has no moving parts, and is insensitive to polarization. Finally, we don't modify the illumination path for multicolor operation, unlike existing SIM implementations[30].

Different implementations of MSIM could improve excitation efficiency or depth penetration. The DMD we used for generating and switching patterns proved highly inefficient. Only a small fraction (<1%) of the pixels were in the ON state during a given raw image, wasting the majority of the excitation light. Using a microlens array in conjunction with a scanning mirror (as in swept-field confocal microscopy) would be far more efficient, and would allow MSIM with existing commercial hardware. MSIM could also use multiphoton excitation (MPE). MPE-based MSIM would result in lower resolution images, due to the longer excitation wavelength, but would limit excitation to the focal plane, reducing out-of-plane bleaching and improving sectioning. Longer wavelengths would also result in less scattering of the excitation and greater penetration into the sample.

## Online Methods

### Illumination System

All optics were mounted on an optical table (Kinetic Systems, Vibraplane Model # 5704-3660-23SPL) to minimize mechanical vibrations. For exciting fluorescence, two lasers were used: a 150 mW, 561 nm laser (561, Coherent, Sapphire 561-150 CW CDRH) and a

200 mW, 488 nm laser (488, Coherent, Sapphire 488-200 CDRH). Mechanical shutters (Thorlabs, SH05 and SC10) placed after each laser were used to control illumination. Beams were combined with a dichroic mirror (DC, Chroma, 525dcxru) and expanded 6.7x with a beam expander constructed from two achromatic lenses (Edmund, f = 30 mm, NT49-352-INK and Thorlabs, f = 200 mm, AC254-200-A-ML). Expanded beams were directed onto a digital micromirror device (DMD, Digital Light Innovations, D4100 DLP 0.55" XGA) 24 degrees off normal, so that in the 'ON' position the micromirrors tilted the output beam normal to the DMD face. The central order of the resulting pattern was demagnified 1.5x with a beam de-expander (Thorlabs, f = 75 mm, AC254-075-A-ML and f = 50 mm, AC254-050-A-ML), aligned in a 4f configuration such that the DMD face was re-imaged at the back focal plane of a 180 mm tube lens internal to the microscope (Olympus, IX-81). These elements are shown in **Supplementary Fig. 3**. After entering the left side port of the microscope, the beam sequentially passed through (i) the tube lens; (ii) a dichroic mirror (Chroma, zt405/488/561); (iii) a 60x objective (Olympus, PlanApo, NA 1.45 TIRF, for single fixed cells, or UPLSAPO 60XS, NA 1.3 silicone oil, for zebrafish, nematode, and live cell samples) for a total demagnification of 90x between DMD and sample. The illumination at the sample covered a circular region approximately 50 μm in diameter. For experiments with the 60x NA 1.45 objective, 488 nm power varied between 2.3 - 25 μW, and 561 nm power between 1.2 - 15.2 μW. For experiments with the 60x NA 1.3 objective, 488 nm power varied between 2.5 - 28.5 μW, and 561 nm power between 1.4 - 17 μW. Power measurements were obtained at the output of the objective.

## Microscope System

SIM imaging was performed on an Olympus IX81 inverted microscope equipped with left and right side ports, and an automated XY stage with an additional Z piezoelectric stage (200 μm range, Applied Scientific Instrumentation, PZ-2000). The patterned excitation created by the DMD was brought into the microscope via the left side port. Fluorescence was collected by the objective, reflected with a dichroic (Chroma, zt405/488/561), passed through a 180 mm tube lens internal to the microscope, filtered appropriately to reject pump light (Semrock, LP02-488RE-25 and NF03-561E-25), and detected with an sCMOS camera (Cooke, pco.edge) mounted on the microscope right side port. Correctly aligning the sCMOS along the optical axis was critical in achieving near diffraction-limited performance. To aid in correct positioning of the camera, we replaced the 60x objectives typically used in imaging with a 10x air objective (Olympus, CPlanFl 10x, 0.3 NA), an optic much more sensitive to errors in axial alignment. We projected a fixed excitation pattern (similar to that used in SIM) onto a fluorescent lake sample (FITC dye sandwiched between two glass coverslips), and translated the camera along the optical axis until the apparent size of each fluorescent spot was minimized.

## Comparative Confocal Measurements

Point-scanned confocal images (**Supplementary Fig. 9**) were acquired using a Zeiss 510 confocal microscope and a 63x Plan-Apochromat (1.4 NA) oil objective. GFP was excited using a 488 nm laser and the emission was collected through a LP 505 nm filter. XY pixel sizes were set to achieve optimal theoretical optical resolution according to Nyquist criteria

for the objective and excitation wavelength used. Inter-slice spacing for z-stacks was set to 200 nm.

### Fixed cellular samples

U2OS cells (a gift from Mike Davidson, FSU) were cultured on ethanol sterilized, cleaned (as described previously[31]) #1.5 25 mm diameter coverslips (Warner Instruments, 64-0715) in standard growth media (DMEM-HG (Invitrogen, 11960), sodium pyruvate (Invitrogen, 11360), GlutaMAX (Invitrogen, 35050) and 10% heat inactivated fetal bovine serum (Invitrogen, 11082)). To stain samples for microtubules, cells were fixed in a mixture of 0.5% glutaraldehyde, 0.37% formaldehyde, and 0.3% Triton X-100 in Cytoskeletal Buffer (CB, 10 mM MOPS, 138 mM KCl, 3 mM $MgCl_2$, 2 mM EGTA, 0.01% $NaN_3$, and 160 mM Sucrose, pH 6.1). After fixation, the cells were washed in CB, quenched with 100 mM glycine in CB, washed in CB, and blocked in antibody dilution buffer (AbDil, 150 mM NaCl, 20 mM Tris, 0.1% Triton X-100, 0.1% $NaN_3$, and 2% bovine serum albumin, pH 7.4). The primary monoclonal antibody (Invitrogen, 32-2500) was diluted to 2 μg/mL in AbDil and incubated with the cells for one hour at room temperature. Following primary antibody incubation, the cells were washed in phosphate buffered saline before incubating them with the secondary, Alexa Fluor 488 labeled antibody (Invitrogen, A-11001) at 1:200 dilution in AbDil for 1 hour.

Samples for dual-color experiments (**Fig. 2**) were initially stained with Mitotracker Red (Invitrogen, M-7512) as per the manufacturer's instructions prior to fixation. After mitochondrial labeling, cells were fixed in 0.5% glutaraldeyde, 0.37% formaldehyde in CB, quenched in 100 mM glycine in CB, and washed in CB. The antibody labeling procedure outlined above was used to stain the microtubules. All samples were mounted in Fluoromount G (Electron Microscopy Solutions, 17984-25) to a standard 25 mm × 75 mm glass slide (SPI supplies, #01251-AB) and sealed with nail polish.

### Live cellular samples

U2OS cells were cultured and transfected with plasmids expressing either GFP-myosin IIA or td-Tomato-F-tractin[32] via electroporation as previously described[33]. A bottom layer of 3 mg/ml collagen I gel was assembled in MatTek dishes[34], using a sufficient volume to generate a 35-45 μm thick gel (confirmed by laser scanning confocal imaging of FITC-labeled collagen I). Cells were adhered to the top of the gel for 30-45 minutes, then encapsulated inside a three dimensional collagen gel by adding additional collagen on top of the cell layer. After adding media (McCoy's medium supplemented with 4 mM L-glutamine, 10% FBS, 10 mM HEPES pH7.4), cells were imaged at 37 degrees C with an objective heater (Bioptechs, 150803 and #150819-13).

### Subdiffractive beads

Yellow-green or red fluorescent beads (Invitrogen, F8803, 110 nm diameter; Invitrogen F8801, 100 nm diameter) were used for all PSF measurements. Beads were diluted from the stock concentration 1:1300 (1:100 in distilled water and 1:13 in ethanol) and spread over cleaned glass coverslips. After air-drying for 5 minutes, to evaporate the ethanol, coverslips were washed twice in distilled water to remove unattached beads. After air-drying again,

beads were mounted in Fluoromount G (for deconvolving datasets displayed in **Figs. 1** and **2**) or silicone oil (for deconvolving datasets in **Figs. 3-5**) onto glass slides, and sealed with nail polish.

## Zebrafish samples

*Tg(XlEef1a1:dclk2-GFP)*$^{io008}$ embryos carrying the zebrafish dclk2-GFP transgene were used in thick MSIM experiments **(Figs. 3** and **4**). To construct this line, plasmids containing the transgene were injected into one-cell zebrafish embryos along with Tol2 mRNA. Fluorescent embryos were raised to adulthood and crossed to select for germline transmission by screening the offspring for GFP expression.

*Tg(XlEef1a1:dclk2-GFP)*$^{io008}$ embryos were collected by natural spawning and maintained at 28°C. Prior to MSIM, embryos at 24 hpf were anesthetized in Tricaine (Sigma, E10521) at a final concentration of 600 μM in embryo media (60 mg RedSea Coral Pro Salt (Drs Foster and Smith Pet Supplies) per liter dd$H_2O$). Anesthetized embryos were mounted on round coverslips, immobilized in 1% low-melt agarose (Cambrex, 50080), placed in a round coverslip holder (ASI, I-3033-25D), covered with embryo media, and imaged at room temperature.

## Worm samples

Strain BV24 [ltIs44 [pie-1p-mCherry::PH(PLC1delta1) + unc-119(+)]; zuIs178 [(his-72 1kb::HIS-72::GFP); unc-119(+)] V] (gift of Zhirong Bao) was raised at 20 °C on NGM media seeded with *E. coli* OP50. Gravid worms were picked from the plate, placed into methyl cellulose, and cut in half to release embryos. Embryos were subsequently transferred to cleaned coverslips, placed in the same holder used for zebrafish experiments, covered with silicone oil (Olympus, Z-81114), and imaged at room temperature. Under these conditions, embryos did not develop past the L1 larvae stage.

## Data Acquisition

Before image acquisition, the onboard memory of the digital micromirror device (DMD) was preloaded with our multifocal illumination patterns. The DMD displayed the patterns in sequence, sending TTL pulses to the camera to trigger exposures. The DMD 'trigger out' signal was high during pattern exposure, and low during the 'OFF' state. We set the DMD to expose each illumination pattern for 2.2 ms, then turned every pixel off for 2.3 ms. We set the camera to expose for 2.2 ms every time it received a trigger pulse. These timing settings enabled the maximum frame rate for a 480 × 480 pixel field of view (4.5 ms/frame, or 222 frames/s), and synchronized illumination and exposure to give the highest signal for a given light dose to the sample. Further details are provided in **Supplementary Note 2** and **Supplementary Note 3**.

## Data Processing

Following acquisition, we processed each set of raw images into a super-resolution image using custom software written in the Python programming language[35]. The processing steps were: *(i)* Automatic lattice detection, to determine the locations of the illumination spots precisely; *(ii)* Digital pinhole masking around each detected illumination spot to reject out-

of-focus light, and optional flat-fielding using calibration data; *(iii)* Local contraction (scaling), resampling the area around each illumination spot to improve the resolution by √2; *(iv)* Summing the processed images to produce an MPSS image; *(v)* Using deconvolution to recover the full 2x resolution enhancement. MPSS methods are described in detail in **Supplementary Note 4**, and our open-source processing code is available at code.google.com/p/msim. The version of the software used to generate the results reported in this manuscript is available in **Supplementary Software**.

### Deconvolution

MPSS datasets were deconvolved using Piotyr Wendykier's Parallel Iterative Deconvolut ion plugin for Image (freely available at http://sites.google.com/site/piotrwendykier/software/deconvolution/paralleliterativedeconvolution). Experimentally measured PSFs (MPSS images of beads, derived either from 110 nm yellow-green beads or 100 nm red beads) were used for 3D deconvolution. For all deconvolution operations, we used the following parameters: Method, Wiener Filter Preconditioned Landweber[36]; Preconditioner, FFT Preconditioner; Tolerance, 0.0; Boundary, Reflexive; Resizing, Auto; Output, Float; Precision, Double; Max number of iterations, 100. On all our datasets, deconvolution converged in < 50 iterations.

## Supplementary Material

Refer to Web version on PubMed Central for supplementary material.

## Acknowledgements

We thank M. Davidson (FSU) for the U2OS cells, Z. Bao (Sloan-Kettering Institute) for the BV24 nematode strain, K. Hazelwood for assistance with cell culture, G. Patterson for the use of his cell culture facilities, and H. Eden, P. Winter, Y. Wu, and C. Waterman for feedback and suggestions on the manuscript. S.H.P. acknowledges financial support from the American Association for the Advancement of Science. This work was supported by the Intramural Research Program of the National Institute of Biomedical Imaging and Bioengineering; the National Institute of Heart, Lung, and Blood; and the National Institute of Child Health and Development.

## References

1. Hell SW. Far-Field Optical Nanoscopy. Science. 2007; 316:1153–1158. [PubMed: 17525330]
2. Betzig E, et al. Imaging Intracellular Fluorescent Proteins at Nanometer Resolution. Science. 2006; 313:1642–1645. [PubMed: 16902090]
3. Rust MJ, Bates M, Zhuang X. Sub-diffraction-limit imaging by stochastic optical reconstruction microscopy (STORM). Nat. Methods. 2006; 3:793–796. [PubMed: 16896339]
4. Hess ST, Girirajan TPK, Mason MD. Ultra-High Resolution Imaging by Fluorescence Photoactivation Localization Microscopy. Biophys. J. 2006; 91:4258–4272. [PubMed: 16980368]
5. Huang B, Jones SA, Brandenburg B, Zhuang X. Whole-cell 3D STORM reveals interactions between cellular structures with nanometer-scale resolution. Nat. Methods. 2008; 5:1047–1052. [PubMed: 19029906]
6. York AG, Ghitani A, Vaziri A, Davidson MW, Shroff H. Confined activation and subdiffractive localization enables whole-cell PALM with genetically expressed probes. Nat. Methods. 2011; 8:327–333. [PubMed: 21317909]
7. Zanacchi FC, et al. Live-cell 3D super-resolution imaging in thick biological samples. Nat. Methods. 2011; 8:1047–1049. [PubMed: 21983925]

8. Shroff H, Galbraith CG, Galbraith JA, Betzig E. Live-cell photoactivated localization microscopy of nanoscale adhesion dynamics. Nat. Methods. 2008; 5:417–423. [PubMed: 18408726]
9. Jones SA, Shim S-H, He J, Zhuang X. Fast, three-dimensional super-resolution imaging of live cells. Nat. Methods. 2011; 8:499–505. [PubMed: 21552254]
10. Hell SW, Wichmann J. Breaking the diffraction resolution limit by stimulated emission: stimulated-emission-depletion fluorescence microscopy. Optics Letters. 1994; 19:780–782. [PubMed: 19844443]
11. Donnert G, et al. Macromolecular-scale resolution in biological fluorescence microscopy. Proc. Natl. Acad. Sci. USA. 2006; 103:11440–11445. [PubMed: 16864773]
12. Rankin BR, et al. Nanoscopy in a Living Multicellular Organism Expressing GFP. Biophys. J. 2011; 100:L63–L65. [PubMed: 21689517]
13. Berning S, Willig KI, Steffens H, Dibaj P, Hell SW. Nanoscopy in a Living Mouse Brain. Science. 2012; 335:551. [PubMed: 22301313]
14. Gustafsson MGL. Surpassing the lateral resolution limit by a factor of two using structured illumination microscopy. J. Microsc. 2000; 198:82–87. [PubMed: 10810003]
15. Heintzmann R, Cremer C. Laterally modulated excitation microscopy: improvement of resolution by using a diffraction grating. Proc. SPIE. 1999; 3568:185–196.
16. Gustafsson MGL, et al. Three-Dimensional Resolution Doubling in Wide-Field Fluorescence Microscopy by Structured Illumination. Biophys. J. 2008; 94:4957–4970. [PubMed: 18326650]
17. Kner P, Chhun BB, Griffis ER, Winoto L, Gustafsson MGL. Super-resolution video microscopy of live cells by structured illumination. Nat. Methods. 2009; 6:339–342. [PubMed: 19404253]
18. Shao L, Kner P, Rego EH, Gustafsson MGL. Super-resolution 3D microscopy of live whole cells using structured illumination. Nat. Methods. 2011; 8:1044–1046. [PubMed: 22002026]
19. Muller CB, Enderlein J. Image Scanning Microscopy. Physical Review Letters. 2010; 104:198101. [PubMed: 20867000]
20. Chitnis AB, Dalle Nogare D, Matsuda M. Building the posterior lateral line system in zebrafish. Dev Neurobiol. 2012; 72:234–255. [PubMed: 21818862]
21. Aman A, Piotrowski T. Wnt/β-Catenin and Fgf Signaling Control Collective Cell Migration by Restricting Chemokine Receptor Expression. Dev Cell. 2008; 15:749–761. [PubMed: 19000839]
22. Nechiporuk A, Raible DW. FGF-Dependent Mechanosensory Organ Patterning in Zebrafish. Science. 2008; 320:1774–1777. [PubMed: 18583612]
23. Paszek MJ, et al. Tensional homeostasis and the malignant phenotype. Cancer Cell. 2005; 8:241–254. [PubMed: 16169468]
24. Nelson CM, Bissell MJ. Of extracellular matrix, scaffolds, and signaling: tissue architecture regulates development, homeostasis, and cancer. Annu Rev Cell Dev Biol. 2006; 22:287–309. [PubMed: 16824016]
25. Engler AJ, Sen S, Sweeney HL, Discher DE. Matrix elasticity directs stem cell lineage specification. Cell. 2006; 126:677–689. [PubMed: 16923388]
26. Pampaloni F, Reynaud E, Stelzer EHK. The third dimension bridges the gap between cell culture and live tissue. Nature Rev Mol Cell Biol. 2007; 8:839–845. [PubMed: 17684528]
27. Hasebe-Kishi F, Shimada Y. Dynamics of actin and alpha-actinin in nascent myofibrils and stress fibers. J Muscle Res Cell Motil. 2000; 21:717–724. [PubMed: 11392553]
28. Mattila P, Lappalainen P. Filopodia: molecular architecture and cellular functions. Nat Rev Mol Cell Biol. 2008; 9:446–454. [PubMed: 18464790]
29. Grotjohann T, et al. Diffraction-unlimited all-optical imaging and writing with a photochromic GFP. Nature. 2011; 478:204–208. [PubMed: 21909116]
30. Fiolka R, Shao L, Rego EH, Davidson MW, Gustafsson MGL. Time-lapse two-color 3D imaging of live cells with doubled resolution using structured illumination. Proc Natl Acad Sci USA. 2012; 109:5311–5315. [PubMed: 22431626]
31. Shroff H, et al. Dual-color superresolution imaging of genetically expressed probes within individual adhesion complexes. Proc. Natl. Acad. Sci. USA. 2007; 104:20308–20313. [PubMed: 18077327]

32. Yi J, Wu X, Crites T, Hammer J. r. Actin Retrograde Flow and Acto-Myosin II Arc Contraction Drive Receptor Cluster Dynamics at the Immunological Synapse in Jurkat T-Cells. Mol Biol Cell. 2012; 23:834–852. [PubMed: 22219382]

33. Pasapera A, Schneider I, Rericha E, Schlaepfer D, Waterman C. Myosin II activity regulates vinculin recruitment to focal adhesions through FAK-mediated paxillin phosphorylation. J. Cell Biol. 2010; 188:877–890. [PubMed: 20308429]

34. Fischer R, Gardel M, Ma X, Adelstein R, Waterman C. Local cortical tension by myosin II guides 3D endothelial cell branching. Curr Biol. 2009; 19:260–265. [PubMed: 19185493]

35. Oliphant T. Python for Scientific Computing. Comput. Sci. Eng. 2007; 9:10–20.

36. Dougherty RP. Extensions of DAMAS and Benefits and Limitations of Deconvolution in Beamforming. AIAA Paper 2005-2961. 2005

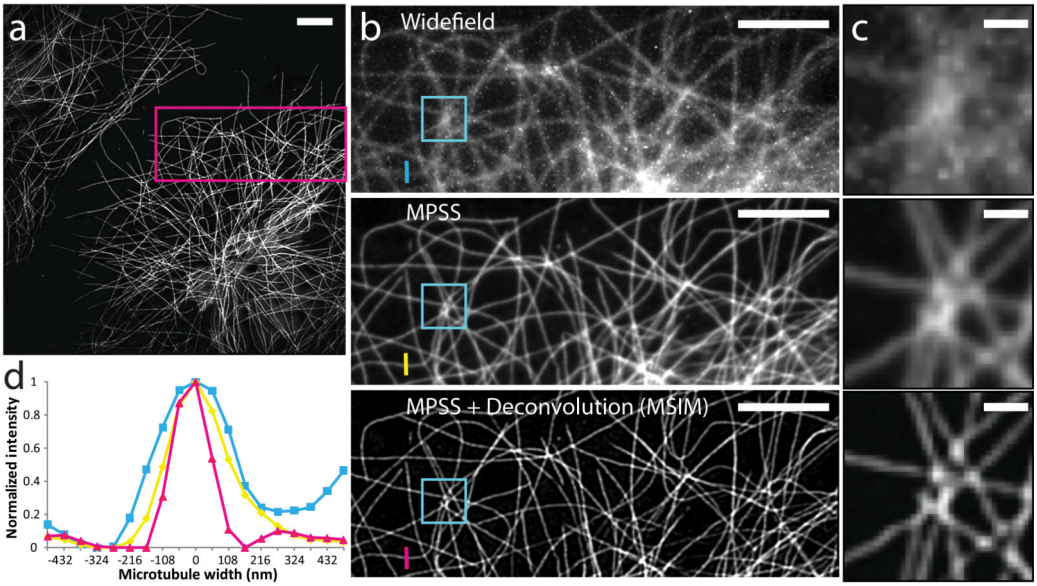


**Figure 1.**

Resolution and contrast enhancement in multifocal SIM. (**a**) Multifocal SIM image of microtubules stained with Alexa Fluor 488 in a fixed cell. The image was generated from 224 raw images, each acquired in 4.5 ms, for an acquisition time of ~1 s. Scalebar 5 μm. (**b**) Higher magnification view of magenta boxed region in (**a**), comparing widefield (top), MPSS image (middle), MPSS + deconvolved (MSIM) image (bottom). Scalebars 5 μm. (**c**) Further magnification of cyan boxed regions in (**b**). Scalebars 1 μm. (**d**) Lineouts of microtubules highlighted with colored bars in (**b**). Full width at half maximum values: widefield 299 nm; MPSS 224 nm; MSIM 145 nm.

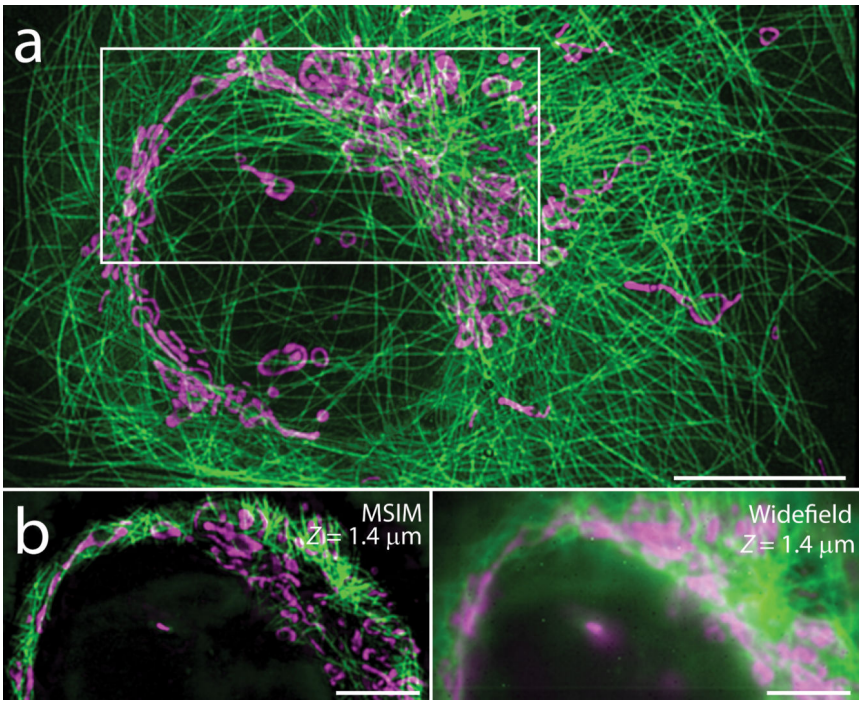


**Figure 2.**

Dual-color, 3D MSIM of a fixed U2OS cell. (**a**) *XY* maximum intensity projection, displaying Alexa Fluor 488 labeled microtubules (green) and Mitotracker Red stained mitochondria (magenta). Scalebar, 10 μm. (**b**) Comparison of the white boxed region in (**a**) between MSIM (left) and widefield (right) slices 1.4 μm from the coverslip surface. The same excitation dose was delivered to the sample in MSIM and widefield mode. Each MSIM slice was generated from 224 raw images, each acquired in 4.5 ms, for an acquisition time of ~1 s per slice, and a volumetric acquisition time of 30 s. Scalebars, 5 μm. See also **Supplementary Videos 2** and **3**.

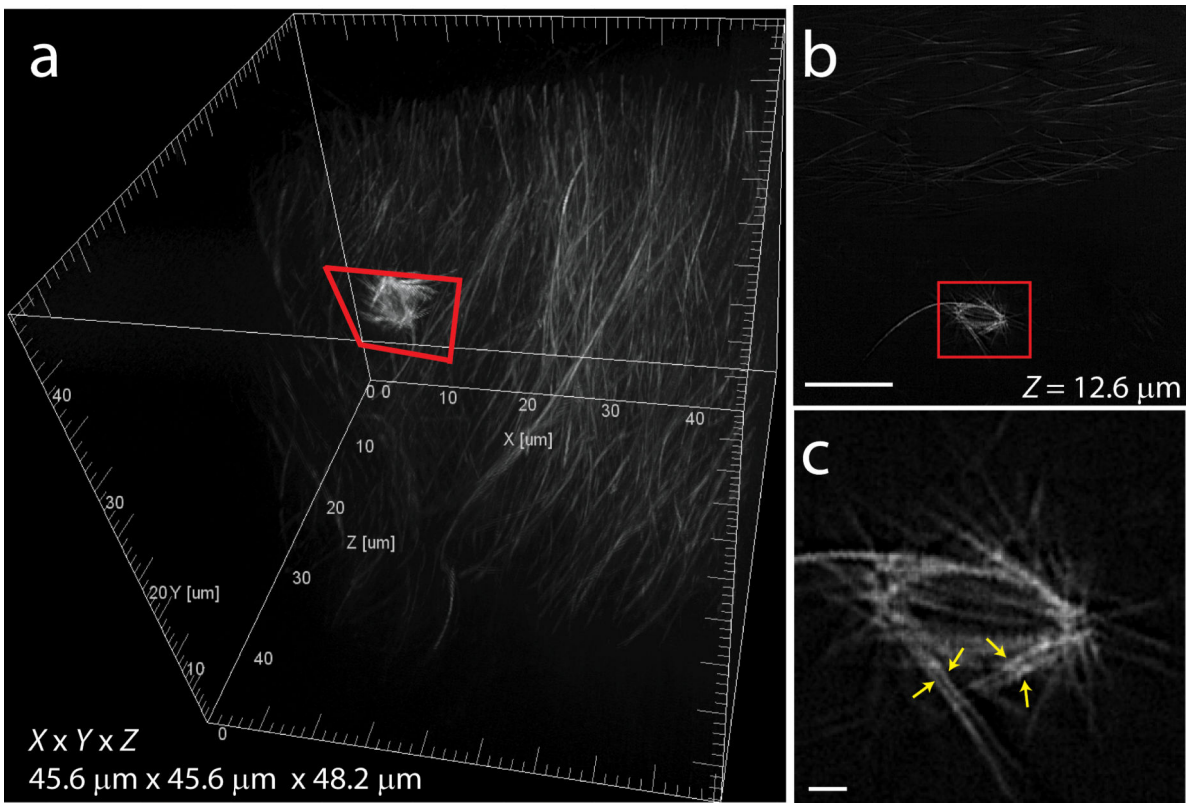


**Figure 3.**

3D MSIM in a live, 24 hpf zebrafish embryo. (**a**) 3D representation of the 45.6 µm × 45.6 µm × 48.0 µm imaging volume, highlighting GFP-labeled microtubules. Red box indicates a dividing cell. (**b**) *XY* slice 12.6 µm into the volume, emphasizing a dividing cell in the epidermis (red box). Scalebar 10 µm. (**c**) Higher magnification view of the dividing cell, yellow arrows highlighting features that are separated by < 200 nm. Scalebar 1 µm. In (**b, c**) the anterior direction is to the left and dorsal to the top. See also **Supplementary Videos 4** and **5**.

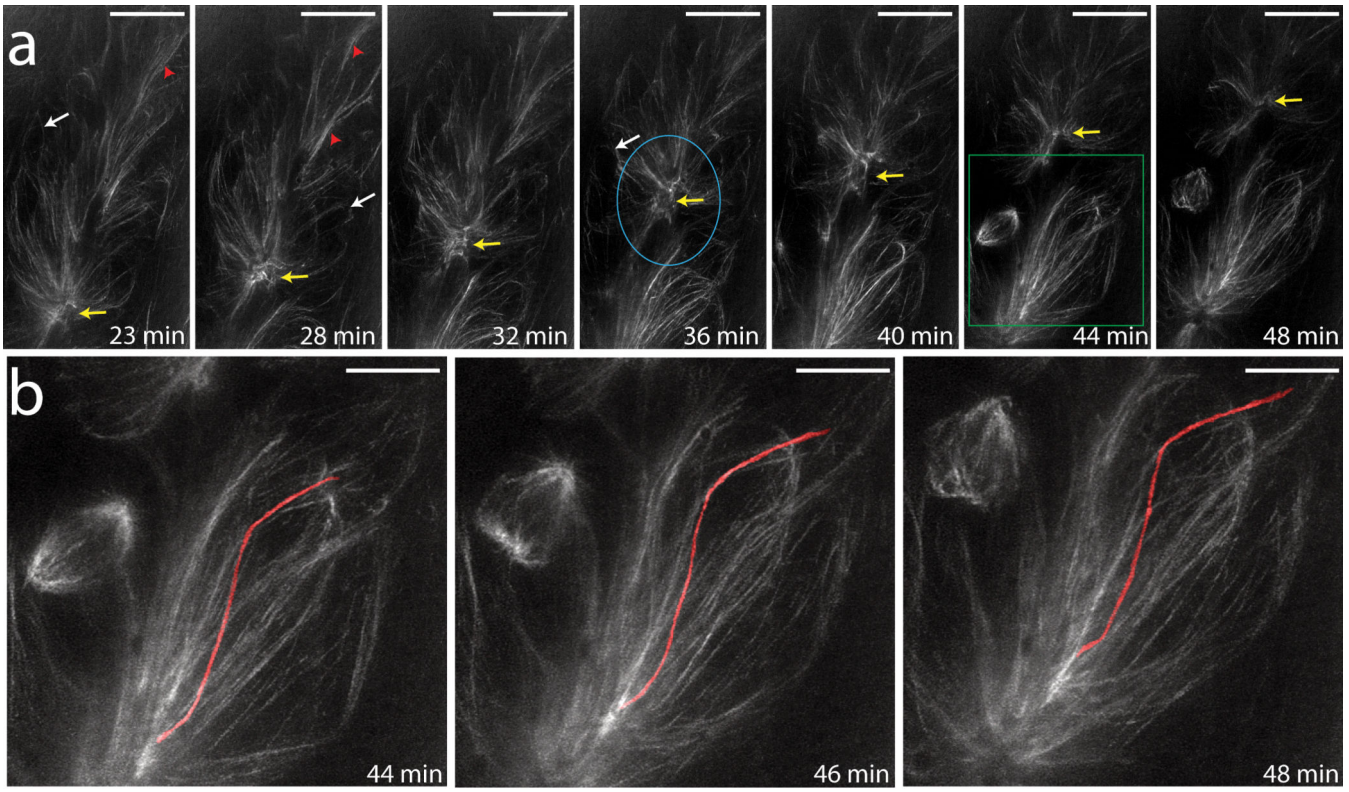


**Figure 4.**

4D MSIM on the posterior lateral line primordium. (**a**) Selected maximum intensity projections composed from the middle 18 slices of each 22 slice volume. White arrows: basal cell bodies enclosed by microtubules; yellow arrows: apical constrictions of a proto-neuromast in a rosette (outlined in blue ellipse) as it moves towards the caudal end of the embryo; red arrowheads: groups of apical midline microtubules in the leading edge of the pLLP. See also **Supplementary Videos 7** and **8**. Scalebars, 10 μm. (**b**) Higher magnification view of green boxed region in (**a**), following a single microtubule (red) from a basal cell body to the apical constriction of a proto-neuromast through selected timepoints. See also **Supplementary Video 9**. Indicated times are relative to the initial time point. Scalebars, 5 μm.

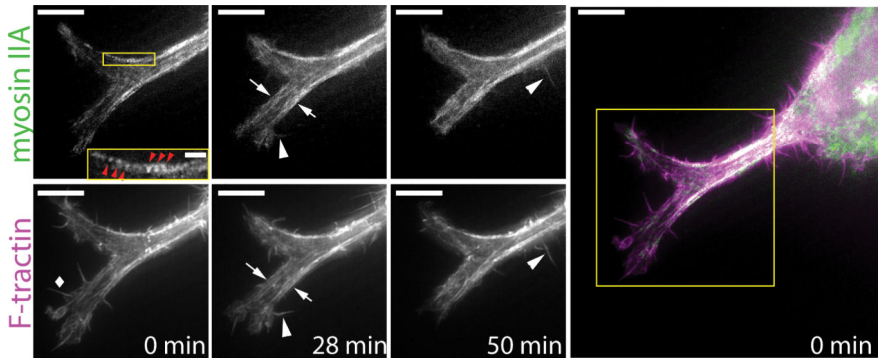


**Figure 5.**

Dual-color 4D MSIM in a collagen gel. Left: Selected time points, showing maximum intensity projections of invadapodium from both GFP-myosin IIA (top row) and td-Tomato-F-tractin (bottom row) channels. Example filapodia (diamond); myosin striations at cell periphery (yellow inset, red arrowheads highlight 350 nm repeat frequency, scale bar 1 μm); actin bundles decorated with myosin (arrows); and retracting filopodia with myosin colocalized at base (arrowheads) are highlighted. Right: Merged view of initial time point. Boxed region corresponds to individual left-hand panels. Scalebars, 5 μm. Indicated times are relative to the initial time point. See also **Supplementary Video 11**.